We are IntechOpen, the world's leading publisher of Open Access books
Built by scientists, for scientists

4,800
Open access books available

122,000
International authors and editors

135M
Downloads

Our authors are among the

154
Countries delivered to

TOP 1%
most cited scientists

12.2%
Contributors from top 500 universities

CLARIVATE ANALYTICS
BOOK CITATION INDEX
INDEXED

WEB OF SCIENCE™

Selection of our books indexed in the Book Citation Index in Web of Science™ Core Collection (BKCI)

Interested in publishing with us?
Contact book.department@intechopen.com

Numbers displayed above are based on latest data collected.
For more information visit www.intechopen.com

8

Retrieving High Resolution 3-D Wind Vector Fields from Operational Radar Networks

Olivier Bousquet
Météo-France, Centre National de Recherches Météorologiques
France

1. Introduction

The ability to retrieve 3-D wind vector fields in a fully operational framework has a potentially wide-ranging impact on a variety of meteorological research and operational meteorological applications. This capability was recently evaluated by the French Weather Service in the course of an upgrade program aiming to introduce Doppler and dual-polarimetric technologies within its radar network. Starting in November 2006, real-time multiple-Doppler wind fields have been produced routinely every 15 minutes for 2 years within a 320x320 km² domain centered on Paris city (Bousquet et al. 2007, 2008a). The evaluation of wind fields synthesized in this framework was carried out from observations collected in a variety of weather situations including low-level cyclones, frontal systems and squall lines. Wind vectors retrieved in the greater Paris area were generally proved very realistic and have been found reliable enough to be used for research applications (mesoscale meteorology, statistical analysis) and numerical model verification (Bousquet et al. 2008b). In order to prepare for the field phase of the international Hydrological Mediterranean Experiment (HyMeX[1]), which will be conducted in 2012-2013, this analysis has later been successfully extended to regions of complex terrain located in the southern part of the country (Bousquet, 2009). The ability to perform operational wind retrieval in mountainous areas is an important step to improve our understanding of orographic precipitation developing in these usually poorly instrumented regions, and also demonstrates that operational real-time wind retrieval could potentially be carried out over the entire French territory – ground elevation exceeds 500 m over ~ 1 fifth of mainland France – which was the initial objective of the French Weather Service when this experiment was started. In 2009, the wind retrieval analysis was therefore extended to the full metropolitan radar network with the goal to implement an operational, nationwide, three-dimensional reflectivity and wind field mosaic to be ultimately delivered to forecasters and modelers, as well as automatic nowcasting systems for air traffic management purposes. In this composite analysis, which is expected to become operational in 2013, data collected by all 24 radars of the French radar network are concentrated, pre-processed and combined in real-time at a frequency of 15 minutes to retrieve the complete wind vector (u,v,w) and

[1] HyMeX is an international program that aims at a better understanding and quantification of the hydrological cycle and related processes in the Mediterranean, with emphasis on high-impact orographic weather events. Information about this program can be found on http://www.hymex.org

reflectivity fields at a horizontal resolution of 2.5 km within a domain of approximately 1000 x 1000 x 12 km^3. This achievement, through the size of the retrieval domain, the number of Doppler radars (24) involved in the analysis, and the fact that retrieved three-dimensional winds rely exclusively on an operational infrastructure, represents an unprecedented breakthrough in operational applications of the Doppler information, which are so far generally limited to clutter filtering and Velocity Azimuth Display analysis (VAD, Browning and Wexler 1968).

The present study aims at examining the technical requirements needed to achieve real-time operational multiple-Doppler analysis in an operational framework, as well as to evaluate the performance and usefulness of three-dimensional wind composite retrieved from operational radar systems. After a recall of the principle of dual-Doppler wind retrieval and a description of the French radar network characteristics winds retrieved in this operational framework are evaluated using outputs produced during various high impact weather events that recently occurred over mainland France. This includes the extratropical storm Klaus, already referred to as the storm of the decade by many European forecasters, which stroke France with hurricane strength winds on 24 January 2009, as well as a heavy orographic precipitation event that occurred over the Massif Central Mountains in September 2010. The potential value of these unique datasets for both operational and a research application is also discussed with emphasis on the upcoming HyMeX program.

2. Wind retrieval

2.1 Principle of dual-Doppler wind retrieval

All current **dual-Doppler** analysis techniques originate from the seminal work of Armijo (1969) who demonstrates that it was possible to retrieve the three components of the wind field in precipitating area using i) the precipitation radial velocity data collected by 2 Doppler radars, ii) the anelastic air mass continuity equation and iii) empirical relationships between radar reflectivity and precipitation fallspeed (Z-R relationships). Among the numerous methods based on Armijo's methodology, three groups can be identified: i) analytical approaches (e.g. Scialom and Lemaitre 1990), which aim at retrieving the wind field under its analytical form, ii) coplane techniques (Lhermitte and Miller 1970, Chong and Testud 1996), which allow resolving the wind field in a cylindrical space and, iii) Cartesian methods, which aim to resolve the wind field in a Cartesian space by the mean of an iterative process between the radial velocity equations and the continuity equation (Heymsfield 1978). Among those 3 families, the latter is the most computationally efficient and the easiest to implement, making it by far the most popular method with researchers.

Despite its relative simplicity, the Cartesian method has nevertheless been an inexhaustible source of inspiration for radar scientists and led to more than 50 peer-reviewed publications over the last 30 years. Although highlighting a particular method among all available Cartesian techniques is difficult, one could mention the approaches proposed by Gamache (1995) – detailed information about this technique can be found in the appendix of Reasor et al. (2009) - Bousquet and Chong (1998) and Gao et al. (1999). All three techniques significantly improved the Cartesian approach by suppressing the iterative process traditionally associated with Cartesian retrieval algorithm (see below).

2.2 The MUSCAT analysis

The wind retrieval technique used by the French Weather Service is the Multiple-Doppler Synthesis and Continuity Adjustment Technique (MUSCAT), which is a variational algorithm allowing for a simultaneous and computationally efficient solution of the three Cartesian wind components (*u, v, w*). This method was originally proposed by Bousquet and Chong (1998) to overcome the drawbacks of iterative analysis techniques used to process data collected by airborne Doppler radars. It was later adapted to ground-based radars (Chong and Bousquet 2001) in order to analyze observations collected during the field phase of Mesoscale Alpine Programme (Bougeault et al. 2001) during which it was used in a semi-operational mode to guide research aircrafts in the field (Chong et al., 2000). The MUSCAT algorithm has been used successfully for more than 10 years in order to synthesize data collected by ground-based and mobile research radars (e.g. Bousquet and Chong 2000, Georgis al. 2003, Bousquet and Smull 2006), and has even been applied to wind lidars (Drechsel et al. 2009). In order to use this algorithm in an operational framework a modification of the initial MUSCAT formalism was proposed by Bousquet et al. (2008a) to take into account extensive radar separation distances prevailing in operational radar networks.

The current form of the MUSCAT algorithm is given hereafter. It consists in a global minimization, in a least-squares sense, of the function F:

$$F(u,v,w) = \int_S \left[A(u,v,w) + B(u,v,w) + C(u,v,w) + D(u,v) \right] dx\, dy \tag{1}$$

such that,

$$\frac{\partial F}{\partial u} \approx 0, \quad \frac{\partial F}{\partial v} \approx 0 \quad and \quad \frac{\partial F}{\partial w} \approx 0. \tag{2}$$

The expression of term *A* is given by:

$$A_{i,j}(u,v,w) = \frac{1}{N} \sum_{p=1}^{n_p} \sum_{q=1}^{n_q(p)} \omega_q \left[\alpha_q u + \beta_q v + \gamma_q (w + v_T) - V_q \right]^2 \tag{3}$$

where *u, v, w,* are the components of the wind field at grid point (*i,j*); V_T is the terminal particle fallspeed at grid point *(i,j)* evaluated from empirical relationships with pre-interpolated radar reflectivity, subscript q defines the q^{th} measurement of a total number n_q that is observed from the p^{th} radar and that falls inside an ellipsoid of influence centered on the grid point (*i,j*); N is the total number of n_q's over the considered domain; ϖ_q is the Cressman weighting function depending on the distance between measurement q within the ellipsoid and the considered grid point; and n_p is the total number of radars covering grid point *(i,j)* (≥ 2).

This term represents the optimal least-squares fit of the observed radial Doppler velocities to the derived wind component. The Cressman distance-dependent weighting function accounts for non-collocated data and grid point values, and allows the interpolation of the radar data onto the Cartesian grid of interest, in the data fit. In the current framework, the interpolation is performed using a fixed horizontal influence radius of the Cressman

weighting function R_H of 3 km and a variable vertical radius of influence R_V that matches the beamwidth of ARAMIS radars.

Term *B* is given by:

$$B(u,v,w) = \mu_1 \left(\frac{\partial u}{\partial x} + \frac{\partial v}{\partial y} + \frac{1}{\rho} \frac{\partial \rho w}{\partial z} \right)^2 \tag{4}$$

where ρ is the air density and μ_1 is a normalized weighting parameter that controls the relative importance of this term with respect to term A.

This term represents the least-squares adjustment with respect to mass continuity. It is formulated for each individual grid box in terms of mass flux throughout the faces of the considered box, which allows solving the wind field over both flat and complex terrains (Chong and Cosma 2000). In this formalism the wind components estimated at the previously investigated plane are used as input values to solve the wind at the current level. In order to initialize the wind synthesis, horizontal components are assumed constant between the surface and the first plane for which the solution for the wind components is searched.

Term C is given by:

$$C(u,v,w) = \mu_2 \left[J(u) + J(v) + J(w) \right]^2 \tag{5}$$

where *J* is a differential operator based on 2nd and 3rd derivatives of the wind components [see Bousquet and Chong (1998) for the detailed expression of this term].

It is a constraint that acts as a low pass filter. Term C allows decreasing small-scale wind variations through the minimization of the second- and third order derivatives. It is controlled by a weighting factor μ_2, which is a function of the cutoff wavelength of the filter. In addition to provide more regular fields, this term is also essential to obtain an objective solution in regions of ill-conditioned analysis through realizing a regular extrapolation in these regions from surrounding properly conditioned areas.

Finally, D is given by:

$$D(u,v) = \mu_3 \left(\frac{\partial (u \sin^2 \alpha_i - v \sin \alpha_i \cos \alpha_i)^2}{\partial x} + \frac{\partial (-u \sin \alpha_i \cos \alpha_i + v \cos^2 \alpha_i)}{\partial y} \right)^2 \tag{6}$$

where μ_3 is given by:

$$\mu_3 = \cos^4 \beta_m \tag{7}$$

and β_m defines the angle between the horizontal projection of the two radar beam axes.

Term D is a constraint that is applied in regions covered by only 2 radars. It allows minimizing the variation of the cross-baseline component of the wind. Its effect is maximum close to the radar baseline and weak in properly conditioned areas (the reader is referred to Bousquet et al. 2008b for more details about this specific term).

According to Equations 3-6, the three-dimensional wind field reconstructed by MUSCAT represents a least squares fit to the available observations and does not perfectly satisfy the mass continuity equation. In order to obtain a wind field that truly verifies this equation, a posteriori upward integration is needed to limit the errors in the vertical component. Many integration methods can be found in the literature to accomplish this last step. For operational applications the basic adjustment technique proposed by O'Brien (1970) was chosen. This method consists in adjusting the vertical velocity by forcing w to be zero at the bottom and top of any column and to linearly distribute the error throughout the column.

3. Operational radar data

3.1 Overview of the French radar network

The French metropolitan operational radar network ARAMIS (Application Radar a la Météorologie Infra-Synoptique) is composed of 16 C-band and 8 S-band Doppler radars. 10 of these radars are equipped with dual-polarization capabilities and we expect the network to be fully polarimetric by 2016. The ARAMIS network covers about 95 % of mainland France with radar baselines fluctuating from ~200 km in the northern part of the country to ~ 60 km in Southeastern France (Fig. 1). It is composed of 5 different types of radars ranging from 25-year old facilities, with limited workload and scanning capabilities, to state of the art dual-polarimetric radar systems. All systems are however equipped with the same radar processor, which allows producing harmonized products despite different hardware characteristics. The French Weather Service, Météo-France, also operates 8 S-band Doppler radars overseas, as well as 2 "gap filling" polarimetric X-band radars in the French Alps. Those 10 additional radars are not considered in this paper.

3.2 The triple PRT Doppler scheme

Doppler capabilities have been introduced in 2002 in the frame of an 8-year upgrade program aiming to modernize the network and fill some gaps in the radar coverage. During this period, all radars have been progressively equipped with the triple pulse rise time (PRT) Doppler scheme proposed by Tabary et al. (2006). This scheme, which is based on the approach proposed by Zrnic and Mahapatra (1985), consists in operating the radars at different pulse repetition frequencies (PRF) in order to mitigate the effect of the "Doppler dilemma" ensuing from the inverse relationship between the unambiguous range and the unambiguous velocity (Doviak and Zrnic 1993). The French scheme yields an extended Nyquist velocity of 60 m s^{-1} up to a range of ~ 250 km. Its particularity lies in the fact that interleaved frequencies are rather low (379, 321, and 305 Hz). This allows this scheme to be indifferently implemented on old and new radars, but also to get rid of potential second trip returns.

The capacity to retrieve multiple-Doppler winds in an operational framework directly arises from the mitigation of the Doppler dilemma. Indeed, one of the main consequences of this long lasting issue is to limit operational Doppler measurements to short range (~ 100 km) so as to mitigate velocity ambiguities resulting from the aliasing of radial velocities outside of the Nyquist interval. Because operational Doppler radars are generally separated by hundreds of kilometers, this limitation in range dramatically impedes overlapping areas where airflow can be successfully reconstructed, and does not allow for adequate dual- or multiple-Doppler wind synthesis.

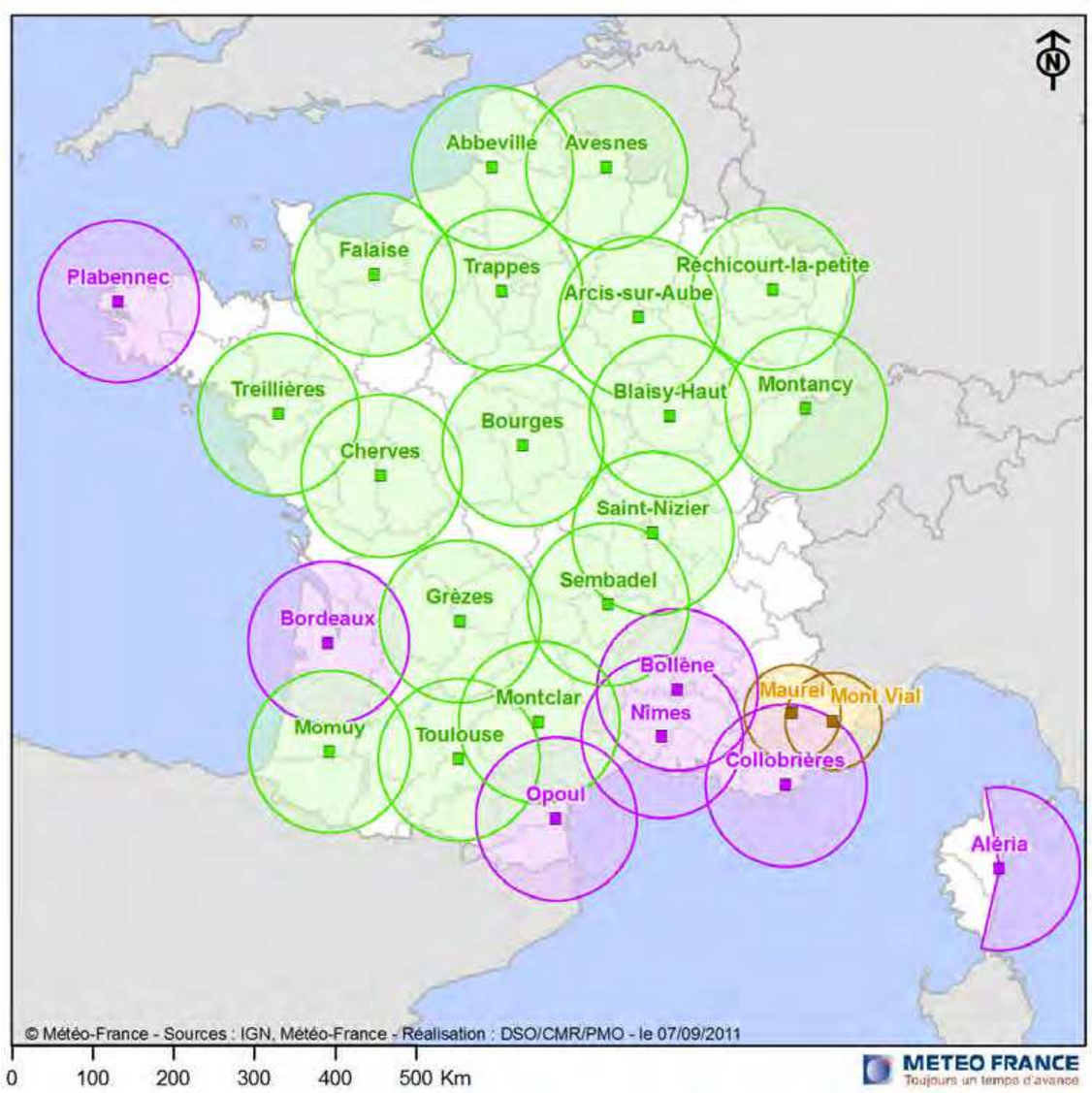

Fig. 1. Map of the French operational radar network ARAMIS. The 100 km (50 km for X-band) ranges of measurement associated with each radar are shown by circles. Green, purple and yellow colors correspond to C-, S-, and X-band radars, respectively.

In France, the ability to measure Doppler velocities at long range allows for a significant dual- and multiple-Doppler coverage over a large part of the country. The resulting coverage is quite heterogeneous due to the principle of ground-based radar measurements and is slightly superior in southern France due to the higher network density in this region. Between a height of 2 and 10 km (Fig. 2a) ~ 90% of the country is covered by at least 2 radar systems. Multiple-Doppler coverage (3 radars or more) is maximized between 2.5 and 9 km altitude, where ~80% of the French territory being covered by at least 3 radars. The radar overlapping near the surface is however quite limited due to both extensive radar baselines and beam blocking by terrain. The detailed maps of radar coverage at 2.5 and 5 km are shown in Fig. 2b-c.

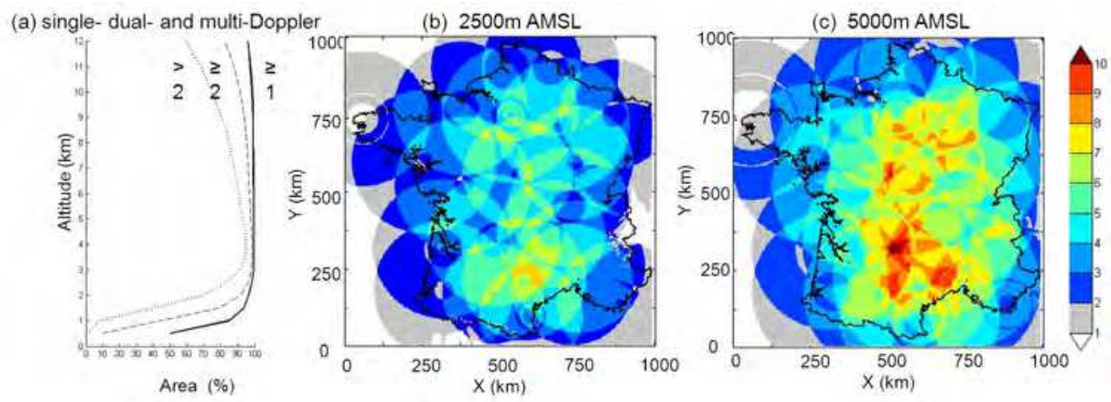

Fig. 2. (a) Radar overlapping within mainland France as a function of height and detailed overlapping map at (b) 2.5 and (c) 5 km AMSL.

3.3 Data processing

Reflectivity and radial velocity observations collected by all (24) ARAMIS radars are concentrated at the national center, in Toulouse, and automatically processed every 15'. Data consist in Cartesian, 512 km x 512 km, 1 km² in resolution, sweeps of radar observations, which are already exploited for current operational applications such as VAD analysis, quantitative precipitation estimates (Tabary et al. 2011) or data assimilation (Montmerle and Faccani 2009). Spurious reflectivity echoes are removed by the mean of a threshold on the pulse-to-pulse fluctuation of the reflectivity based on the work of Sugier et al. (2002). A 5x5 km² median filter is then applied to radial velocity measurements to discard potential spurious velocities resulting from dealiasing failures (Tabary et al. 2006). Finally, data are synchronized with respect to the ending time of the 15' sampling period to account for the non-simultaneity of the measurements following the approach of Tuttle and Foote (1990). Once pre-processed, data are ingested in the MUSCAT analysis described in Section 2.

4. Examples of retrieved wind fields

A qualitative evaluation of the multiple-Doppler winds reconstructed in this framework is provided through the analysis of radar data collected during various rain events that occurred over mainland France between 2008 and 2010. This includes the extratropical cyclone Klaus, which stroke France on 24 January 2009 with hurricane force gusts, and a number of orographic convective precipitation events that produced large amount of rain over the Massif Central Mountains.

4.1 Extratropical cyclone "Klaus"

4.1.1 Overview

On 24 January 2009, an extratropical cyclone called "Klaus" made landfall over southwestern Europe with hurricane force gusts, causing widespread damage and many fatalities, especially across France and Spain. This event is considered the most intense storm affecting Western Europe since the infamous extratropical cyclones "Lothar"

(Wernli et al., 2002) and "Martin" in 1999. The heaviest damages occurred in southern France where millions of homes and commercial properties experienced power cuts and heavy damages due to falling trees. In Northern Spain and Southwestern France some of the most productive European forests have been profoundly impacted by the storm and will likely take decades to recover. In the French Landes department for instance, one estimates that 70 % of the pine forest – this forest, the largest of this kind in Europe, was accounting for about one third of France's lumber production - has been completely wiped in just a few hours.

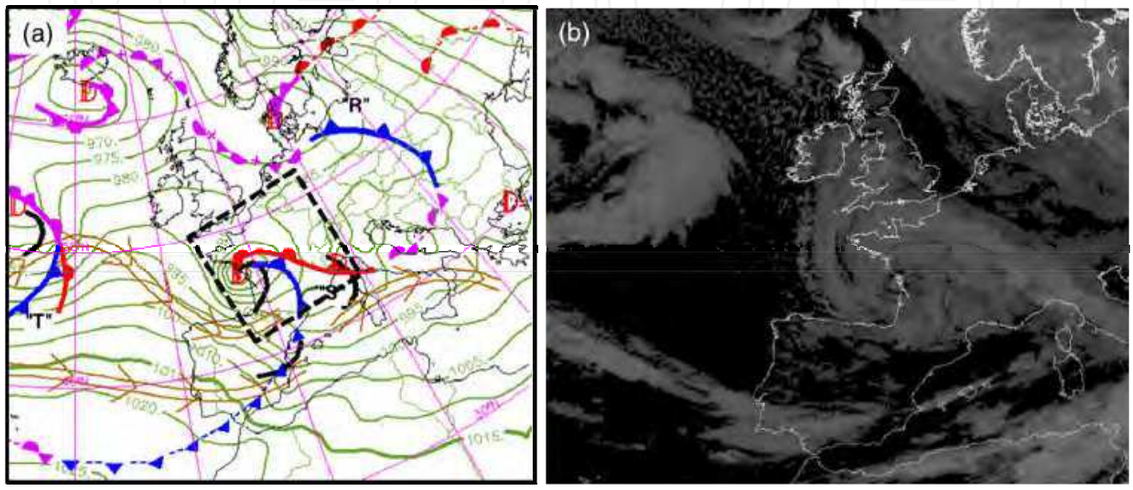

Fig. 3. (a) Surface analysis and satellite imagery over Western Europe valid 24 January 2009 at 6 UTC. The black square in (a) shows the area where wind retrieval is performed.

Klaus formed west of the Azores islands on 23 January 2009 near 00 UTC and made landfall about 30 hours later after crossing the Atlantic Ocean at a mean speed of 27 $m.s^{-1}$. The life cycle of this system approximately follows the conceptual model proposed by Shapiro and Keyser (SK, 1990). It is characterized by an explosive intensification period, during which the sea level pressure (SLP) at the cyclone center deepened by ~ 36 hPa in 24 hours, ending up with a warm seclusion phase and a rapid decay. The SLP minimum (964 hPa) was reached at 00 UTC, 24 January, as the low-level vortex was located ~ 400 kilometers off the French coasts. Klaus made landfall slightly before 6 UTC on 24 January near Bordeaux, France (Fig. 3) with a minimum pressure of ~ 967 hPa (Fig. 4). The corresponding surface analysis (Fig. 3a) shows a warm frontal zone to the North of the cyclone center and a cold front extending far southward across the Pyrenees and Northern Spain. According to satellite images (Fig. 3b) the storm was elongated in the west-east direction along the warm front, which is in good agreement with the SK model theory (Schultz et al. 1998). After landfall, the system progressed eastward at a mean speed of about 15 $m.s^{-1}$ and reached Italy near 18UTC (Fig. 4). At this time the associated minimum pressure has already increased to 988 hPa. Maximum surface winds occurred in a region located approximately 300 to 350 km south of the cyclone center, along a 100 km swath oriented in a direction almost parallel to the cyclone trajectory. In France, wind gusts peaked at ~ 184 $km.h^{-1}$ near Opoul (Fig. 1), a value corresponding to category 3 hurricane winds on the Saffir-Simpson scale. The situation was even more impressive in Northern Spain where surface wind gusts over 200 $km.h^{-1}$ have been recorded at several locations.

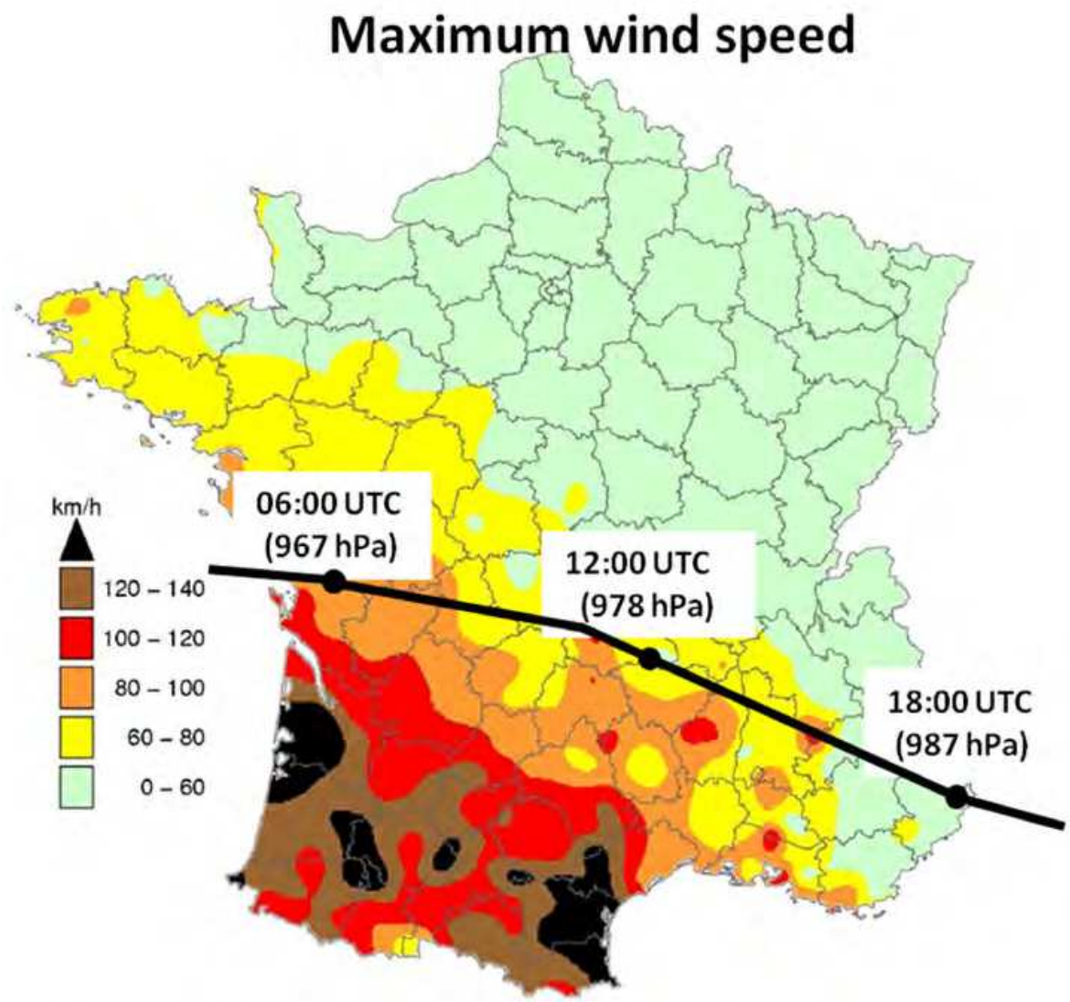

Fig. 4. Recorded maximum surface wind speed during the passage of Klaus over France. The trajectory and central pressure of the cyclone are also indicated.

4.1.2 Radar-derived wind and reflectivity fields

Observations collected between 03 and 9 UTC on 24 January 2009 are shown in Fig. 5 All radars performed nominally during this period with the exception of the Momuy radar, which was forced to cease operations near 05UTC due to heavy wind damages. Velocity data recorded just before the radar failure were in excess of 60 $m.s^{-1}$ (216 $km.h^{-1}$) at 2000m MSL and ~ 45 $m.s^{-1}$ (160 $km.h^{-1}$) close to the ground. Also note that the French radar network was not yet completely Doppler-ized at this time resulting in some gaps in the dual-Doppler radar coverage over northwestern and southern France.

Figure 5 presents horizontal cross-sections of wind and reflectivity fields over France at 2 km MSL and different stages of the storm evolution. At 3 UTC (Fig. 5a-b), a large part of the country was already affected by weak to moderate precipitation. The most intense rainfall occurred approximately 300-400 km in advance of the cyclone center along a SW-to-NE oriented rainband that marks the location of the cyclone associated cold front. Another area of intense precipitation associated with the cloud head (Browning 1999) could also be identified farther west. Both regions of intense precipitation were separated by an area of weaker precipitation associated with the dry intrusion identified in Fig.5a. Relatively intense winds in the range of 25- 30 $m.s^{-1}$ could already be observed in the southeastern France (east of the cold front) and within the cloud head.

According to radar data, Klaus made landfall ~ 3 hours later near the city of Nantes (Fig. 5c-d). The closed circulation associated with the cyclone center can be clearly identified in Fig 5c. The diameter of the vortex deduced from radar observations was about 350 km. Severe winds reaching up to 50 $m.s^{-1}$ have already penetrated deeply over land as seen by the patch of very intense winds located ~400 km of the cyclone center from each side of the dry slot. The location of this area of particularly strong winds is in good agreement with surface observations (Fig. 4). One can also notice the presence of several thin rainbands located to the west of the wind maximum, within the cloud head. This banded structure is consistent with that described by Browning (2004) and suggests the existence of multiple mesoscale slantwise circulations, which may have played an active role in strengthening the damaging winds (the investigation of processes at play during this event is outside the scope of this study). After landfall the patch of strong winds stretched out along a NW-SE axis more or less parallel to the orientation of the Pyrenees mountain chain and slowly progressed southeastward towards the Mediterranean coast. Strong winds remained active during the entire period. A wind maximum of up to 55 $m.s^{-1}$ could be observed west of the Toulouse radar at 09UTC (x ~ 400 km, y ~ 200 km) in good agreement with surface observations (Fig. 4).

As there is currently no way to collect wind measurements at the space-time resolution achieved by ground-based Doppler radars, the validation of such operational wind data is extremely difficult. In order to evaluate these results, we propose to compare retrieved radar winds with those analyzed by the French operational numerical weather prediction system ALADIN (Aire Limitée Adaptation Dynamique Développement International; Radnóti et al. 1995). ALADIN is a limited area regional model that covers France and part of Western Europe at the horizontal resolution of 10 km. The comparison between radar-derived and analyzed horizontal winds at 1.5 km MSL at 6 UTC is shown in Fig. 7. Overall, the location of the cyclone center, the dimension of the vortex, and the intensity and direction of the winds at mid-level appear quite similar in both analyses. Some discrepancies can yet be seen along frontal boundaries (the wind shift associated with the cold front is for instance slightly more marked in the radar analysis) and to the North of the Massif Central Mountains, about 500 km east of the cyclone center. In the latter area the model produces a pronounced zonal wind component that is apparently not resolved in the radar analysis. This pronounced southerly component was nevertheless missing in all 15' analyses produced between 4 and 8 UTC. Although no strong conclusions can be inferred from this observation, this temporal consistency of the wind field may plead for an error in the analysis rather than in the retrieved winds.

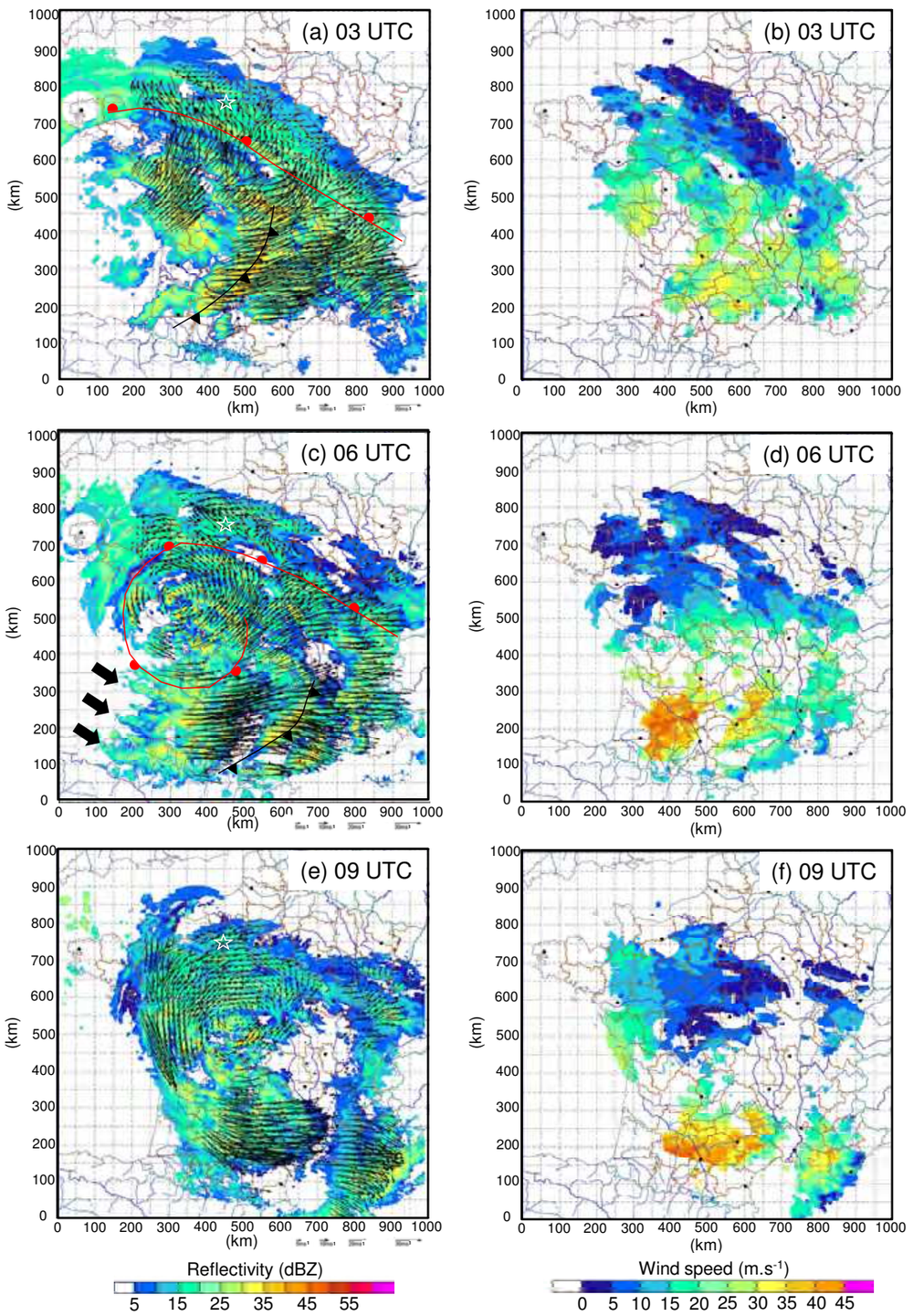

Fig. 5. 3-hourly multiple-Doppler analysis of radar data over France starting at 03 UTC on 24 January 2009. Left panel shows reflectivity (dBZ) superimposed on horizontal wind vector at 2.5 km AMSL. Right panel shows horizontal wind speed (m/s). One every sixth vector is plotted. Frontal boundaries deduced from surface analysis are shown in (a) and (c).

4.2 The 7 September 2010 "Cevenol" event

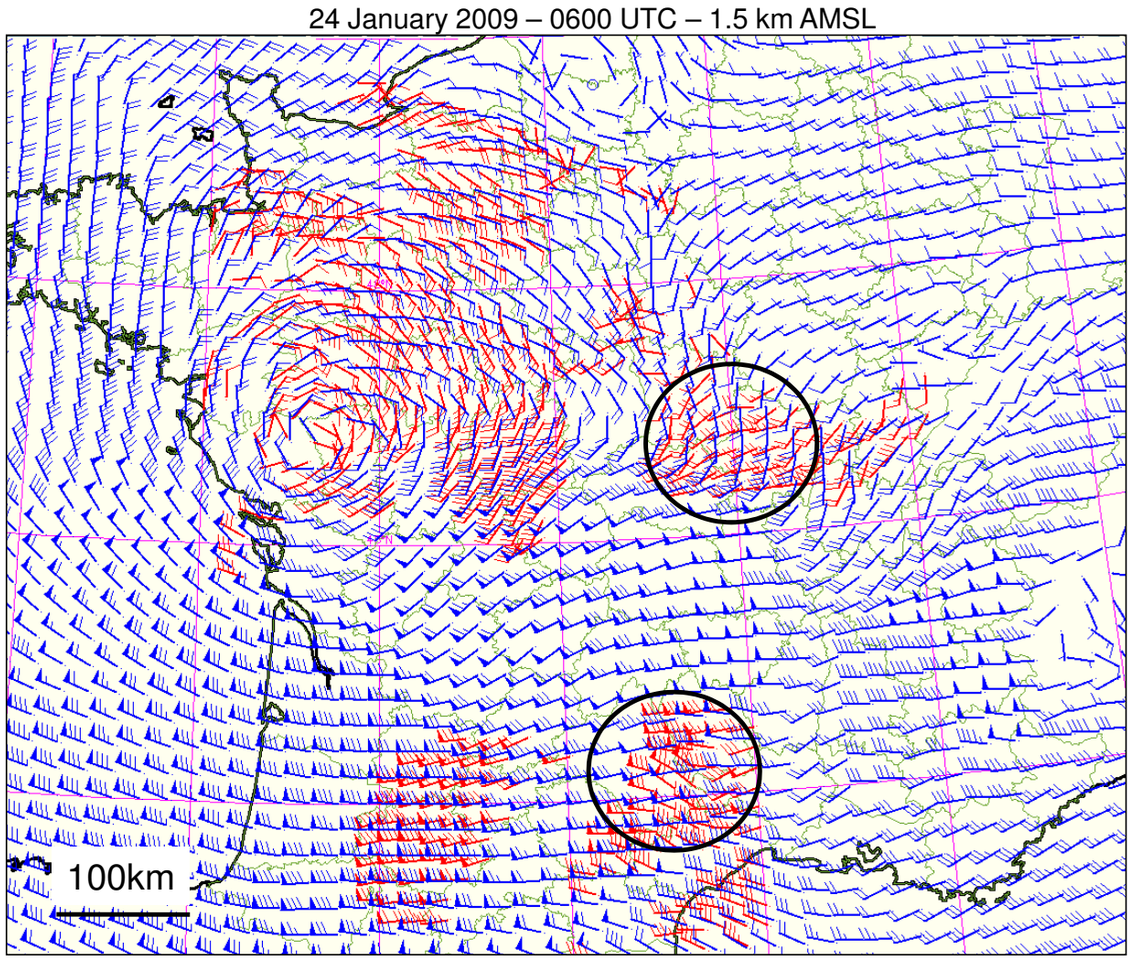

Fig. 6. Comparison between ALADIN operational (blue) and radar-derived winds (red) at 1500 AMSL on 24 January at 6 UTC. Black circles show area where the 2 analyses significantly differ.

4.2.1 Overview

During the fall season, the southeastern region of France is often affected by intense flash-flooding episodes ensuing from the formation of quasi-stationary mesoscale convectivesystems along the south-eastern flank of the Massif Central Mountains (Cevennes region). These systems can generate considerable amount of precipitation in relatively short periods of time. A well-known example of such systems is the so called "Gard case" (Delrieu et al. 2005) during which ~ 800 mm of rain fell down in less than 24 hours over the French Gard department, resulting in many fatalities and total damage amount of about 1.2 billion US dollars. Observing and understanding the dynamical and to some extent microphysical processes at play during these high impact weather events is critical to develop effective flood warnings systems and to improve their forecast. In the following we present examples of radar analyses produced during a heavy precipitation event that

occurred in the Nimes area on 7 September 2010. Although this storm did not generate major damage, it locally produced rainfall accumulation in excess of 300 mm in just a few hours.

The 500 hPa analysis at 12 UTC, 7 September 2010 is shown in Fig. 7. Note that at this time convection over the Gard department has already started and was already well established. The upper level analysis indicates the presence of an upper-level cold low centered over the British Islands with an associated trough extending southward toward the Iberian Peninsula. This synoptic pattern generates a mid-to-upper level southwesterly flow over France and a low-level southerly flow over the Mediterranean Sea veering slightly south-easterly near the French coast.

The corresponding Deutscher Wetterdienst (DWD) low-level analysis (Fig. 8b) shows a surface low centered over Ireland and a main front extending meridionally through central France ahead of the trough which attained France on the 6 September (Fig. 8a). A secondary front can also be noticed a few hundred kilometers west of the main front, over the Atlantic Ocean. The latter is associated with a low-pressure anomaly located slightly north of the Spanish coast. In the following hours (Fig. 8c-d), this front and its associated surface low propagated rapidly eastwards to ultimately catch up with the leading front. The low surface pressure anomaly reached Western France by 18 UTC (Fig. 8c) and rapidly extended over a large part of the country (Fig. 8d).

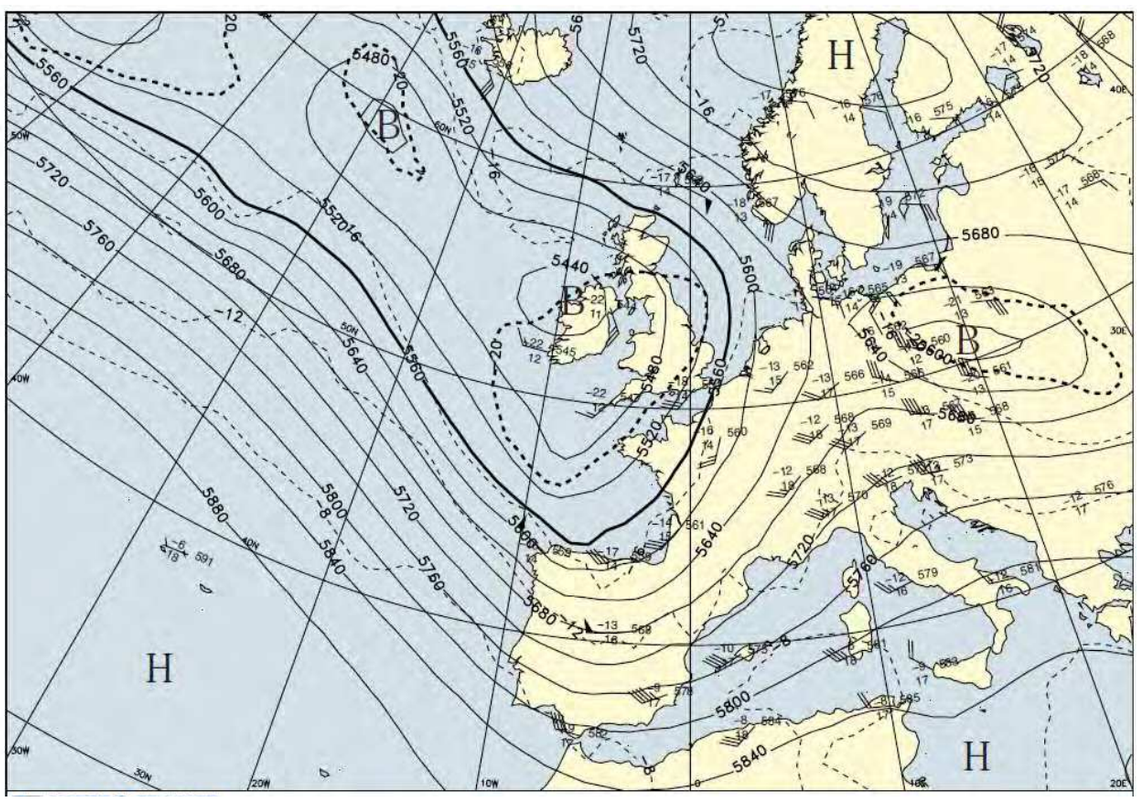

Fig. 7. Operational analysis of geopotential height at 500 hPa valid on 7 Sept 2010 at 12 UTC.

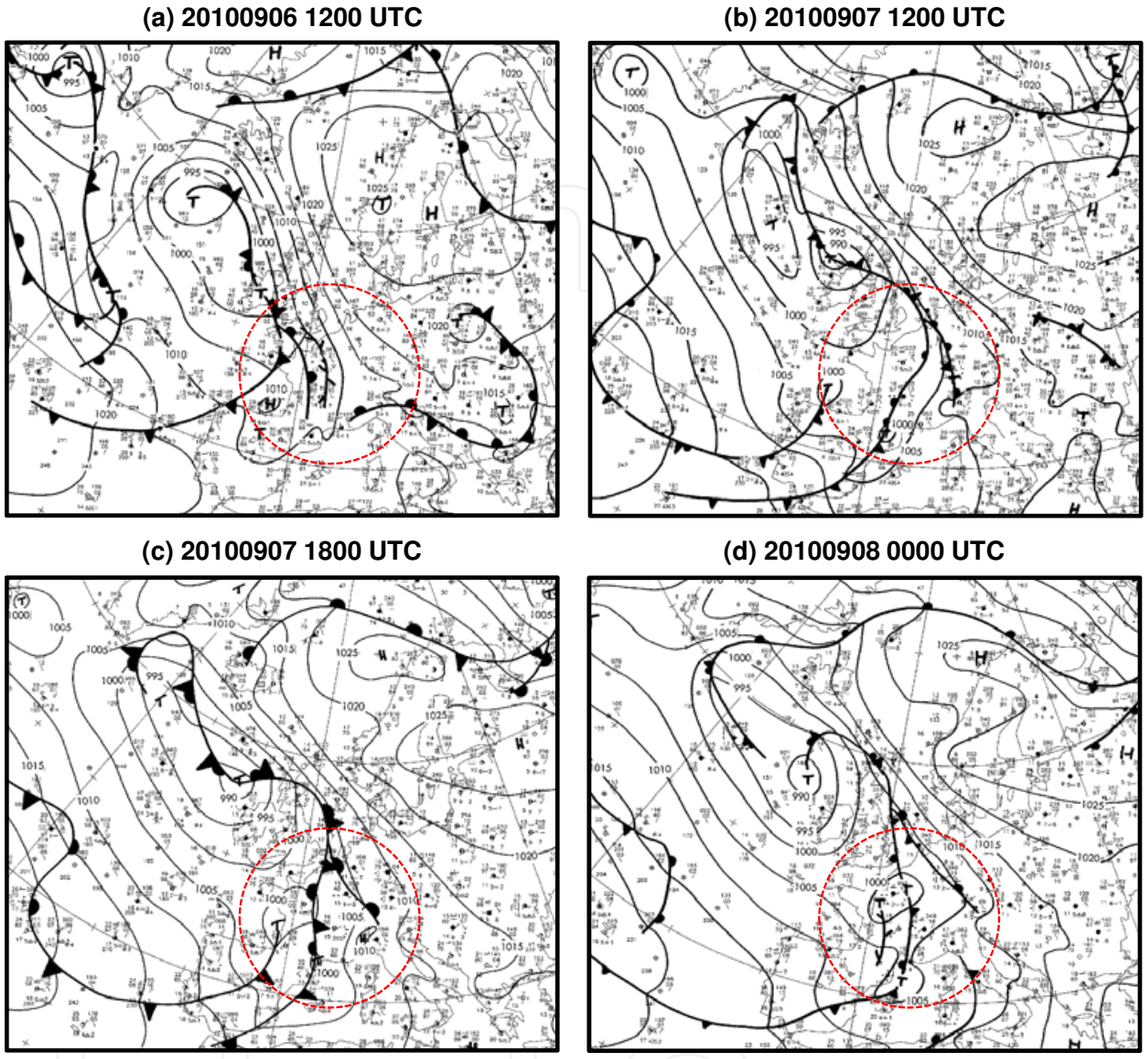

Fig. 8. DWD operational surface analyses valid at (a) 12 UTC 06 Sept 2010, (b) 12 UTC 07 Sept 2010, (c) 18 UTC 07 Sept 2010, and (d) 00 UTC 08 Sept 2010. The red circle indicates the area where multiple-Doppler wind retrieval is performed.

The 24-hour accumulated precipitation pattern (Fig. 9) shows a pronounced maximum of ~300 mm over the Gard department. The maximum rainfall amount was recorded close to the foothills of the Massif Central in the city of Conqueyrac where 308 mm of precipitation felt in 7 hours. Significant rainfall also occurred over the Massif Central as indicated by a well-defined band of accumulated precipitation in the range of 75-150 mm. This pattern is consistent with the slow propagation of the leading surface front noticed in Fig. 8 and suggests that frontal perturbations have been slowed-down and possibly enhanced by the Massif Central Mountains.

4.2.2 Radar-derived wind and reflectivity fields

Figure 10 presents multiple-Doppler analysis of radar data produced every 6 hours from 12 UTC, Sept 6 to 00 UTC, Sept 8 at a height of 2.5 km (left panel) and 6 km (right panel). The composite reflectivity patterns (right panel) show extensive frontal rainbands propagating eastwards in good agreement with the surface analyses shown in Fig. 8. Starting from 18 UTC, 6 September (Fig. 10c), one can notice the presence of widespread convective cells over southeastern France and northern Spain that seem to be triggered by the pronounced relief of the Pyrenees. These cells, which develop in a southwesterly midlevel level flow, are advected northeastwards towards the Massif Central Mountains before eventually aggregating into a stationary mesoscale convective system (MCS) along the flank of the mountains. The retrieved wind circulation at both 2.5 and 6 km altitude shows relatively uniform southwesterly wind, except near the Massif Central where the mid-level flow exhibits a more pronounced southerly component. This southerly flow, which tends to advect warm and moist air masses from the Mediterranean Sea toward the coast, impinges on the Massif Central Mountains and is responsible for the enhancement of convection over

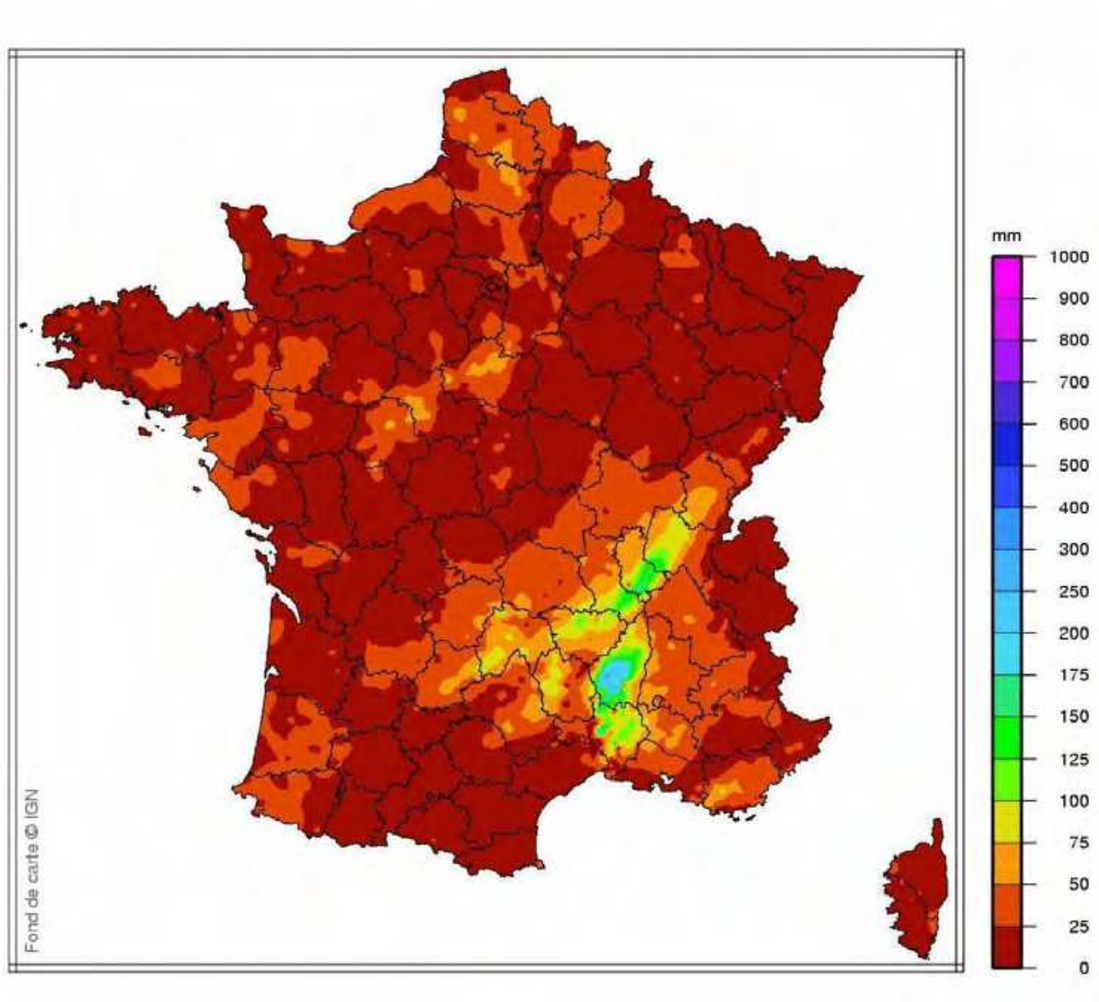

Fig. 9. 24-h accumulated precipitation (mm) over France starting at 00 UTC, 7 Sept 2010

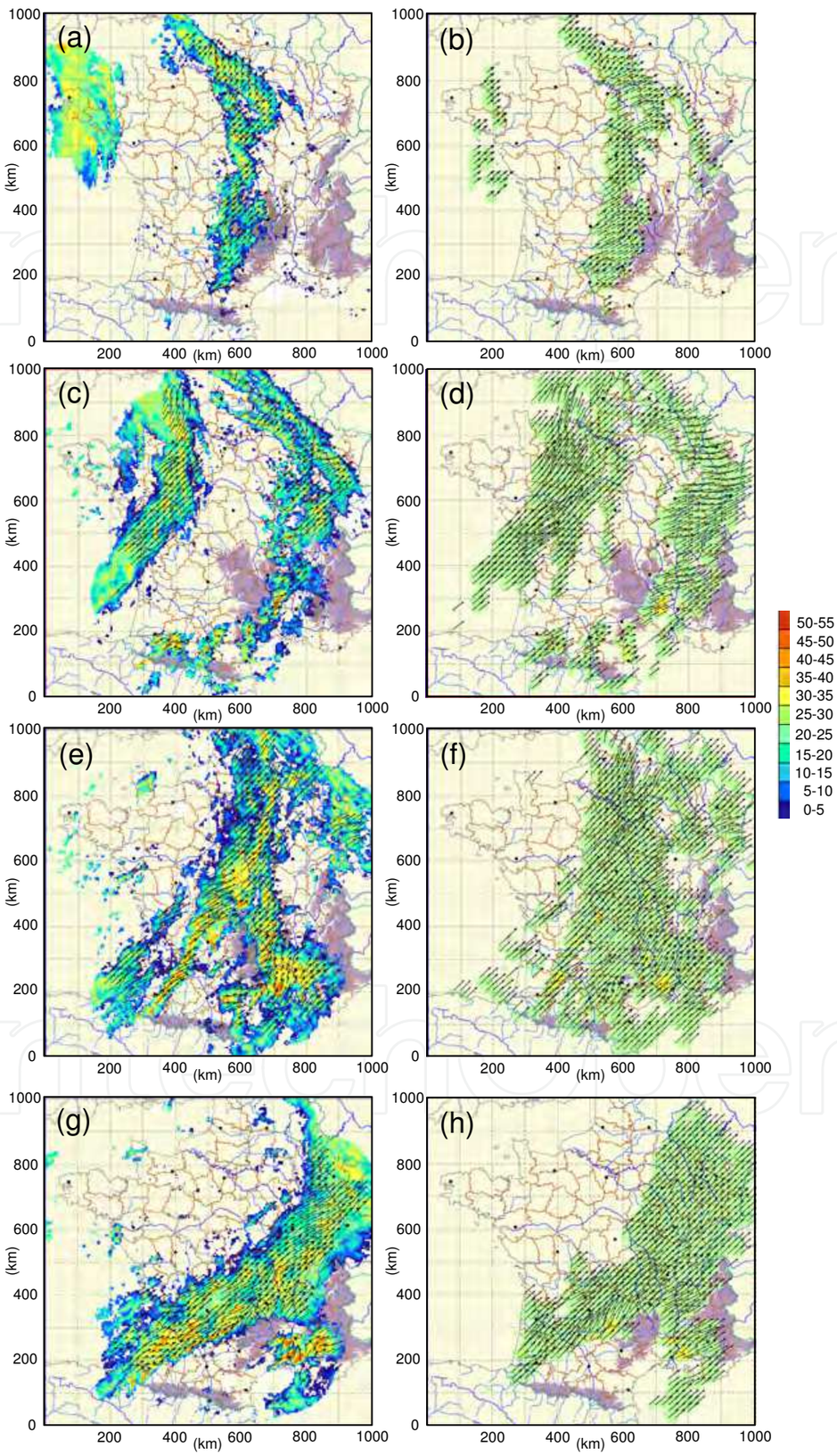
(a)
(b)
(c)
(d)
(e)
(f)
(g)
(h)
(km)
0
200
400
600
800
1000
50-55
45-50
40-45
35-40
30-35
25-30
20-25
15-20
10-15
5-10
0-5

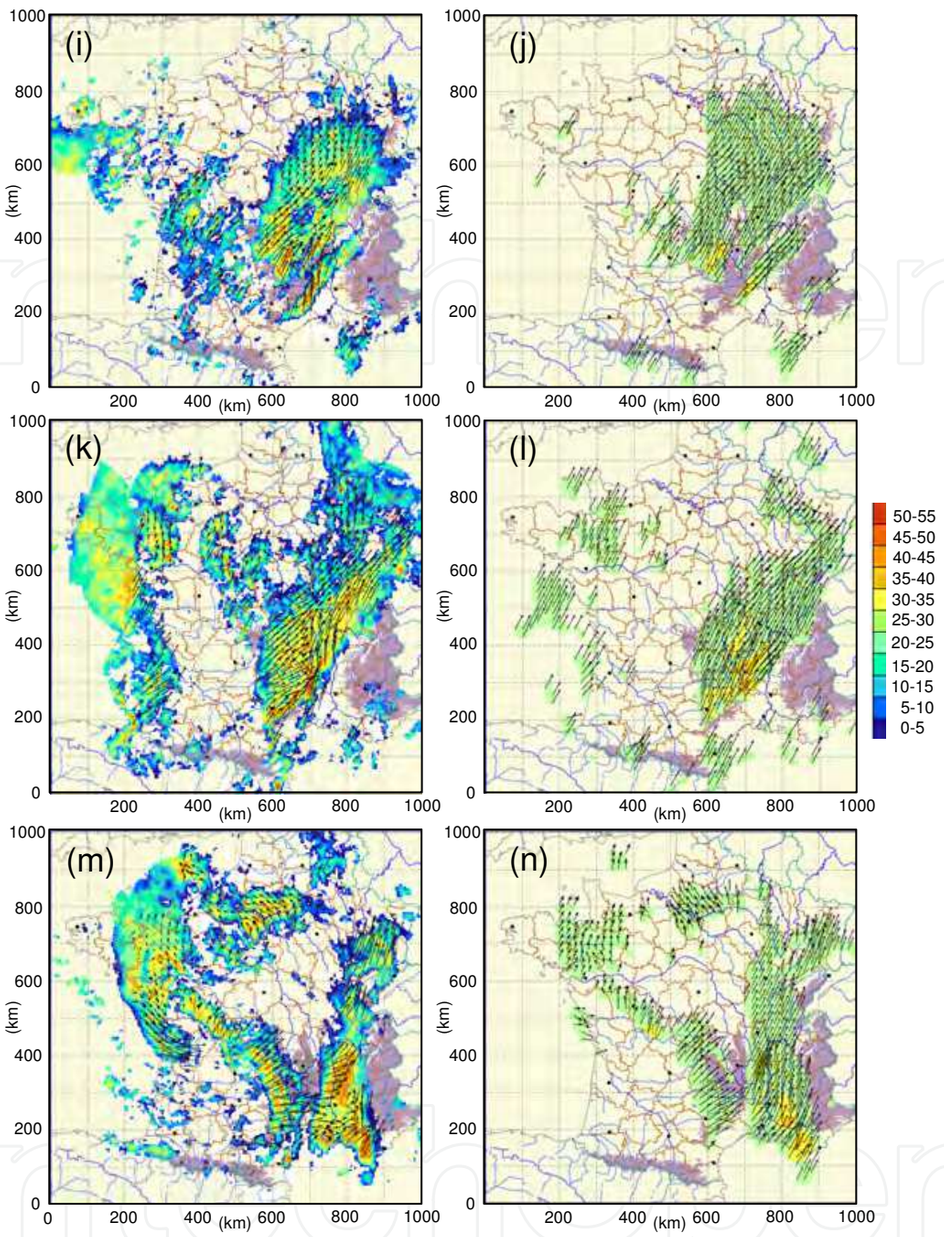

Fig. 10. 6-hourly multiple-Doppler analysis of radar data over France starting at 12 UTC on 6 Sept 2010. Left panel shows reflectivity (dBZ) superimposed on horizontal wind vector at 2.5 km AMSL. Righ panel shows vertical velocity (m/s) and horizontal wind vectors at 6 km AMSL. Vertical velocity values (m/s): dark green ($w<-1$) green ($-1\leq w<1$), yellow ($1\leq w<2$), orange ($w\geq 2$). One every sixth vector is plotted.

the Cevennes area. The convective activity in this region significantly intensified in the following 12 hours (Fig. 10e and g), as shown by radar reflectivity values increasing up to 55 dBZ. During this period, the MCS also became more organized and developed a well-defined stratiform region. At 12 UTC, 7 September, the MCS was absorbed by the frontal

rainband associated with the cold front that had been moving across France for ~ 24 hours (Fig. 10i). The various interactions between air masses occurring during the merging process seemed to reinforce the convective activity along the southern flank of the Massif Central. The most intense convection was hence observed around 18 UTC (Fig. 10k).

In order to better understand the processes at play in the Cevennes region, Fig. 11 presents a zoomed view of low and midlevel flow at 00 and 21 UTC, 7 September within a 400 x 400 km² domain centered on Nimes. At 00 UTC (Fig. 11c), the low-level flow impinging on the Massif Central was from the SE and was oriented in a direction almost perpendicular to the mountains. The maximum convection was observed slightly off the slopes. This is likely due to the presence of a cold pool below the system, which acted to displace the triggering effect of the mountains farther south (cold dome effect; Reeves and Lin 2005).

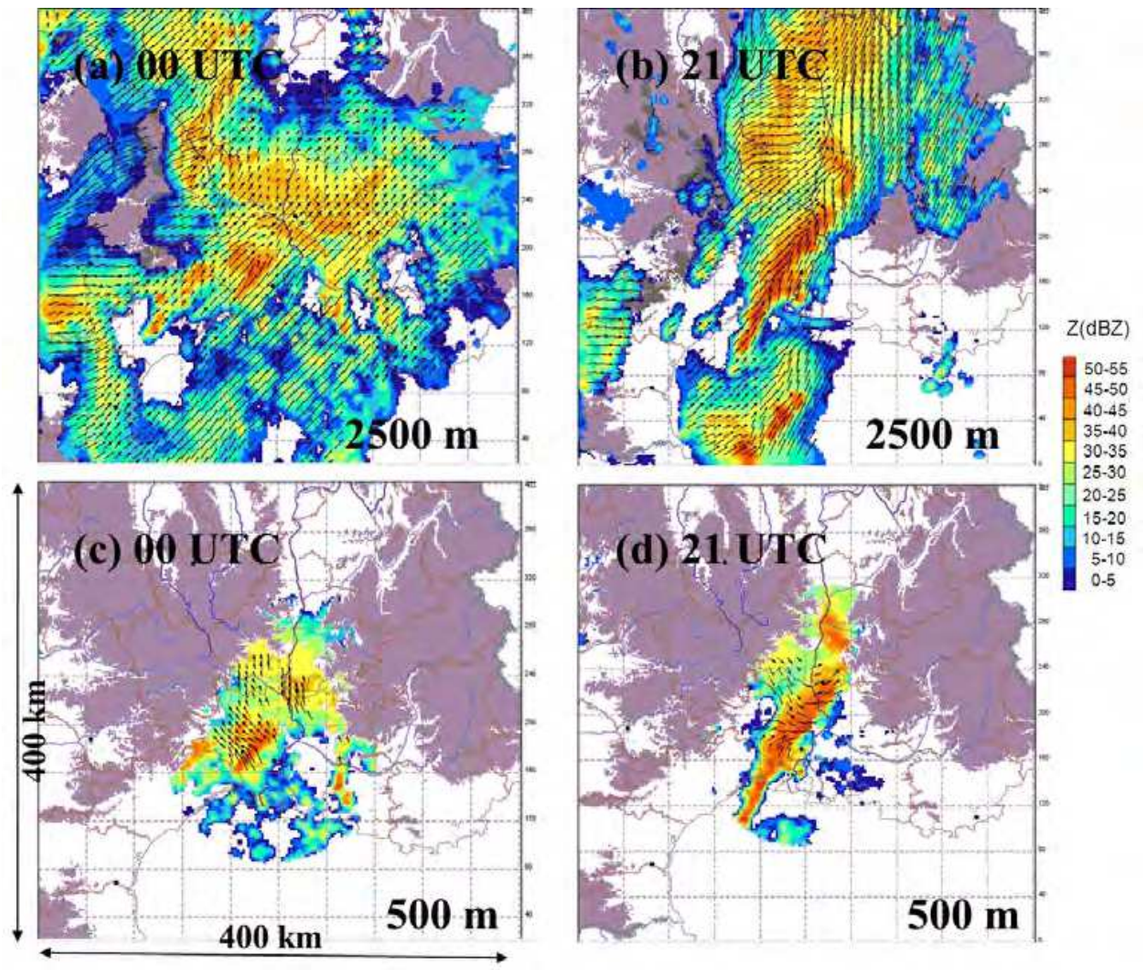

Fig. 11. Multiple-Doppler analysis of radar data within a domain of 400 km x 400 km centered near Nimes, France valid at 00 UTC and 21 UTC, 7 Sept 2010. Upper panels shows reflectivity (dBZ) superimposed on horizontal wind vector at 2.5 km AMSL. Lower panels shows panel shows reflectivity (dBZ) and horizontal wind vectors at 500m AMSL. Grey shading indicates Massif Central (left) and Alps (right) mountain chains. One every fourth vector is plotted.

At 21 UTC, one can note a profound reversal of the incident upslope-oriented flow, resulting in the formation of a northwesterly flow over the slopes of the Massif Central. Such pronounced return flow has already been observed over the Alps in the frame of the MAP experiment from airborne and mobile radar systems in response to negative buoyancy generated by both melting and evaporation of precipitation particles below the 0^{o} C isotherm (Bousquet and Smull 2003, Steiner et al. 2003). The process generating the observed downslope flow by cooling from melting and evaporation of precipitation particles in the Massif Central is likely similar to that observed over the Alps in the late nineties. This is supported by the fact that stratiform precipitation lasted for several hours over the mountains before the formation of this downslope circulation (Fig. 10g,i,k). In this particular case, however, it seems that the downslope flow has had a strong impact on the convective activity by triggering new cells in the Rhone valley (Fig. 11d), whereas its effect was not found significant in previous studies.

After the merging, the frontal system remained blocked over the Massif Central and the eastern part of France for about 12 hours during which another 100 mm of rain felt over the Cevennes area. It finally passed the Cevennes near 00 UTC, 8 September as it was swept away by another frontal system approaching from the West. At this time, the low surface pressure anomaly identified in Fig. 8c had reached the French territory and had started to extend over a large part of the country. The associated cyclonic circulation (Fig. 10m) was well captured by the French radar network.

More information about the vertical structure of precipitation can be inferred from Fig. 12, which presents 6-hourly meridional cross-sections of the retrieved 3D composite reflectivity pattern along a 1000 km line ranging from the Golfe du Lion, in the Mediterranean Sea, to Belgium. These cross-sections provide a unique picture of the structure and evolution of precipitation over the entire country and can be very useful to quickly identify regions of intense rainfall, as well as to segregate between frontal and more convective precipitation. This time series, extending from 00 UTC to 18 UTC on 7 September, thus confirms that convection became significantly more intense after the frontal system reached the Massif Central Mountains. At 12 UTC (Fig. 12c) and 18 UTC (Fig. 12d) one can see that very deep convection was thus occurring over the Cevennes and the Rhone valley with convective cells reaching up to 35 dBZ at a height of 11 km.

In addition to horizontal wind fields, the MUSCAT analysis used by the French weather service also allows to retrieve accurate vertical velocities in the whole precipitating area within the 1000 km x 1000 km domain of analysis. Retrieved vertical motion fields at a height of 6 km, which is the altitude at which maximum vertical motion was observed, are displayed in Fig. 10. Overall, one can note a very good consistency between the location/intensity of updrafts and the position of the most active convective cells (left panel). Upward vertical motions are the most intense after the MCS has merged with the frontal rainband that is the moment when low level convergence was the most important. This observation is consistent with the vertical structure of precipitation deduced from Fig. 12 that indicates the presence of deep convection and shows a particularly impressive vertical extension of the convective cells.

During the Klaus storm, getting real-time or quasi real-time information about wind intensity would have been particularly useful to forecasters in order to trigger or cancel alerts, as well as to precisely monitor the propagation of the strong wind swath. On September 7 2010, a watch was ongoing for heavy precipitation and flash flood in the Cevennes area but forecasters were more interested in getting high resolution radar quantitative precipitation estimates in order to assess the hydrological risks.

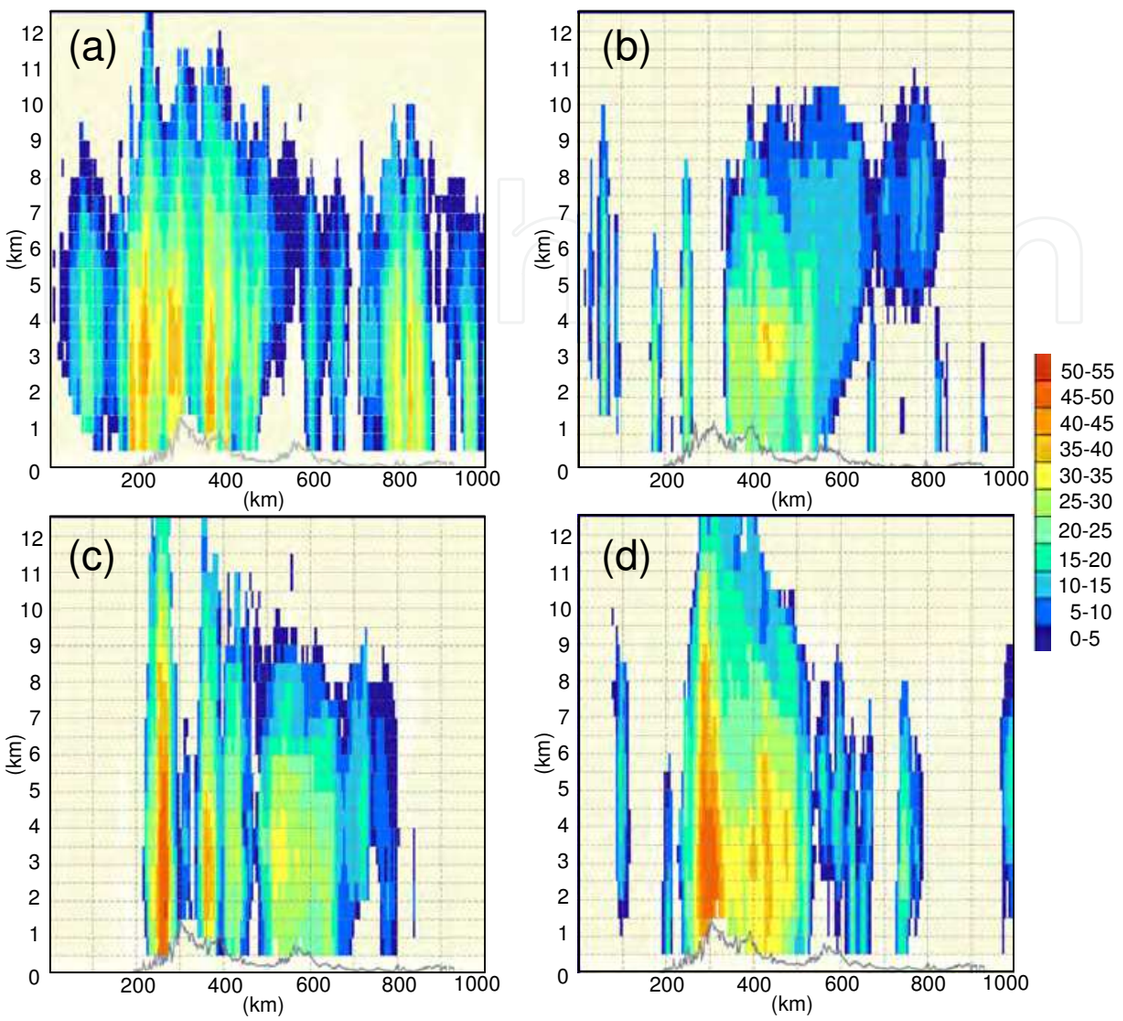

Fig. 12. Vertical cross-section of radar reflectivity (dBZ) at x=700 km (Fig. 10) at (a) 00 UTC, (b) 6 UTC, (c) 12 UTC and (d) 18 UTC on 7 Sept 2010.

Wind observations would nevertheless have been quite useful to anticipate the behavior of convective cells, especially in the Rhone valley where the intensity of the convection seemed directly related to the direction and strength of the wind. On the other hand, the benefit inferred from such products for research purposes is priceless. These wind fields could be used to develop new methods for model verification as well as more efficient nowcasting tools. Radar-derived wind information produced in a fully operational framework (i.e., in real time and automatically) could also be relied upon to evaluate numerical model output in real time (through identifying possible temporal or spatial phase shift in model output), as well as to build a weather database that would be used for statistical analysis purposes or more traditional case studies. Such capabilities, for instance, are at the heart of the upcoming HyMeX field phase, which will be held in Sept-Nov 2012.

4.3 20-22 October 2008 MCS Cevenol precipitation event

The last example consists in an isolated MCS (Fig. 13a) that developed along the south-eastern flank of the Massif Central Mountains on October 20th and remained stationary for about 15 hours. Again, this storm did not generate any significant damage, but it locally produced rainfall accumulation in excess of 250 mm in a just a few hours.

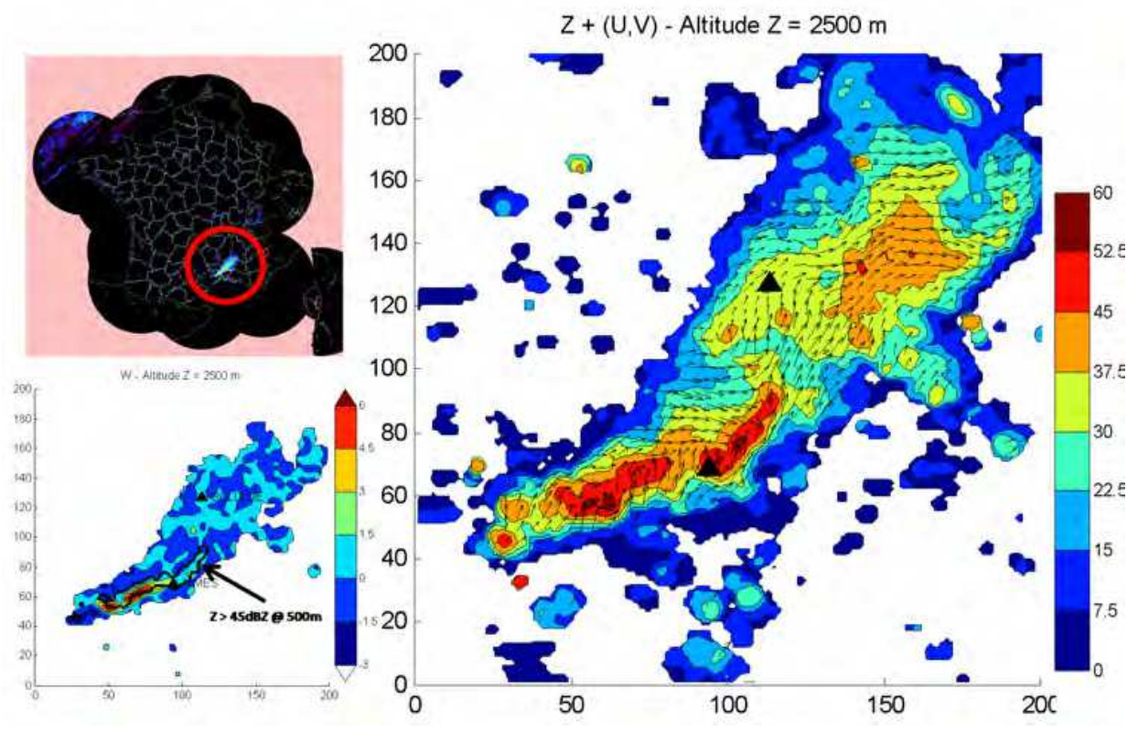

Fig. 13. Stationary mesoscale convective system observed on 20 October 2008 at 14 UTC. (Left, top): French operational radar reflectivity mosaic output. (Right): Horizontal wind vectors superimposed on radar reflectivity (shaded) at 2.5 km MSL within the 200 km x 200 km experimental domain, as derived from multiple-Doppler analysis of radar data. (Left, bottom): Associated retrieved vertical velocity. Triangles show the location of Nimes and Bollène radars. One every sixth vector is plotted.

The retrieved wind and reflectivity fields associated with this MCS at 14 UTC are shown in Fig. 13b within a domain of 200 x 200 km centered between the Nimes and Bollene radars (black triangles) at a horizontal resolution of 1 km. Note that only 4 radars (Bollene, Nimes, Montclar and Collobrieres, see Fig. 1) are used in this analysis. This setup will be used to produce high resolution wind fields in real-time during the first phase of the HyMeX program in fall 2012. Radar-derived wind and reflectivity fields will be used to guide both research aircraft and ground-based mobile radars systems towards the most interesting areas. Overall, the radar analysis shows a rather complex wind circulation resulting from the interactions between the incident flow originating from the Mediterranean Sea and the terrain. A region of strong convergence was observed near Nimes due to the interactions of westerly flow in the southern part of the massif with southerly-to-southwesterly flow to the east. As a consequence, strong convection could be observed in this region while more

stratiform precipitation, associated with older cells, could be seen to the North. The vertical velocity field (Fig. 13, bottom right) in the convective region also shows intense updraft up to 8 m/s, which is consistent with observed reflectivity cores up to 60 dBZ. Note that retrieved vertical velocities were significantly higher than those retrieved within the 7 September 2010 system due to the much higher horizontal resolution of the wind field (1 km vs. 2.5 km).

A new precipitation event occurred over the same area the day after as a new stationary MCS formed at about the same location, along the southern flank of the Massif Central Mountains (Fig. 14). This time, however, the situation was quite different as a rainband associated with a southeastward propagating cold front merged with the isolated MCS at the end of the day and eventually swept it away. In essence, this new event is thus relatively similar to the 7 Sept 2010 case described previously. Figure 15 shows the evolution of the MCS between 0 UTC and 8 UTC on the 22nd of October. This time series begins slightly after the frontal system reached the Massif Central. The location of the cold front can be identified by the wind shift seen at both low and mid-levels. Note that the strong low-level southerly flow impinging on the barrier at 0 UTC quickly weakened as the front approached the eastern flank of the Massif, which acted to cut the feed of moisture originating from the Mediterranean Sea and prevented the formation of new convective cells. Convection over the area thus died very quickly and the MCS was rapidly swept away by the cold front. A major difference with the 2010 case is that the frontal system did not remain blocked over the relief and stratiform precipitation over the slopes thus only lasted for a short period of time. This is likely the reason why no reversal flow could be observed over the slopes of the Massif Central on this day as the cooling resulting from melting and evaporation of precipitation particles, which is responsible for the formation of the downslope flow, was not sufficient for this phenomenon to occur.

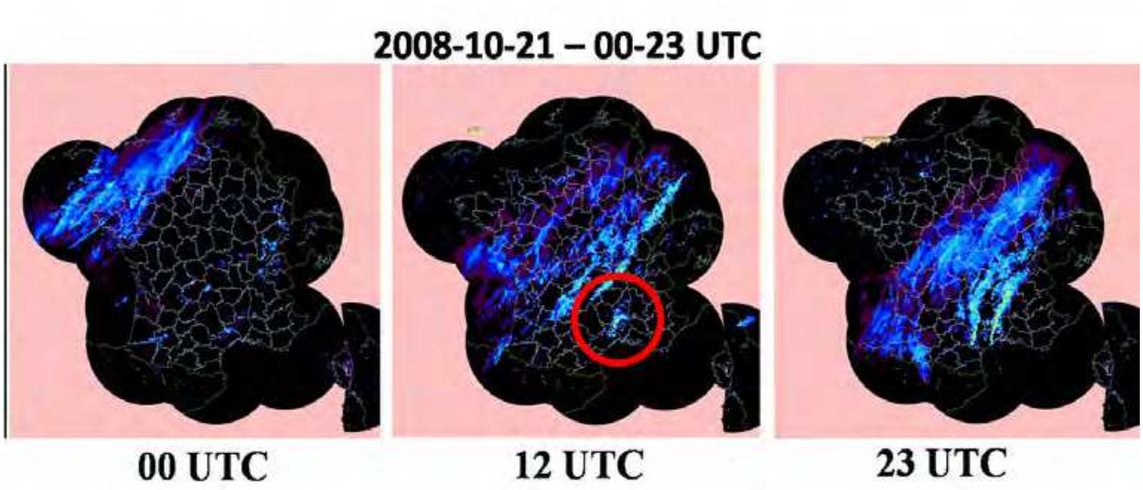

Fig. 14. French operational radar reflectivity mosaic outputs on 21 October 2008 at 00, 12, and 23 UTC. Red circle indicate the location of the isolated MCS.

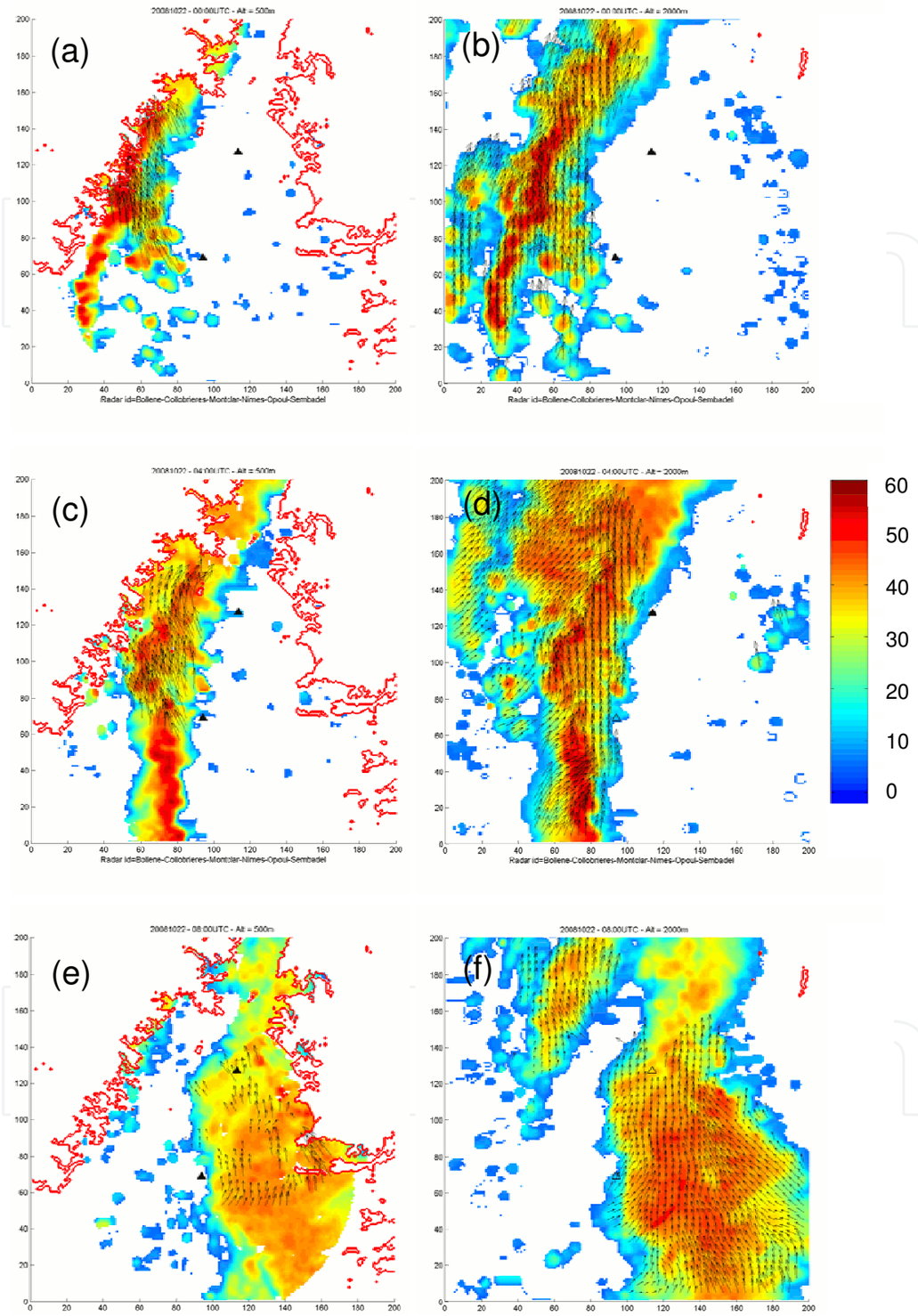

Fig. 15. Horizontal wind vectors superimposed on radar reflectivity (shaded) at 0.5 km (left panel) and 2.0 km (right panel) AMSL within a 200 km x 200 km experimental domain, as derived from multiple-Doppler analysis of radar data at (a,b) 00 UTC, (c,d) 04 UTC and (e,f) 08 UTC on 22 October 2008. One every sixth vector is plotted.

5. Conclusion

The ability to collect Doppler measurements up to long range resulting from the recent deployment of a new triple-PRT scheme within the French radar network ARAMIS allows to mitigate the Doppler dilemma and to achieve extensive multiple-Doppler coverage while collecting high quality radial velocities. This achievement brings new perspectives in terms of exploitation of operational Doppler measurements such as the ability to perform multiple-Doppler wind synthesis in a fully operational framework. In this context the French weather service has started to produce a new mosaic of wind and reflectivity covering the entire French territory. Reflectivity and radial velocity observations collected by the 24 ARAMIS radars, which are concentrated at the national center in Toulouse, are synthesized every 15' to produce a nationwide, three dimensional, wind and reflectivity composite.

An evaluation of multiple-Doppler wind fields synthesized in this framework was carried out from data collected during several weather situations characterized by fundamentally different airflow and precipitation regimes that is, the extratropical cyclone Klaus that stoke France with hurricane strength winds on 24 January 2009, as well as several heavy orographic precipitation events that occurred over the Massif Central Mountains in 2008 and 2010. Airflows retrieved at different horizontal resolutions ranging from 2.5 to 1 km are highly consistent with those documented earlier from high resolution research radar data, which suggests that multiple-Doppler winds retrieved in this operational framework are definitely reliable. Wind and reflectivity fields produced routinely in this framework are archived since about a year and are already available to researchers from many countries. This product will be used in a quasi-operational mode (real-time) to guide mobile research systems and evaluate numerical model outputs during the field phase of the Hydrometeorological Cycle in the Mediterranean Experiment (HyMeX) to be held in southern France in fall 2012. It should become fully operational near year 2013 after having been thoroughly evaluated by the forecasters of the French Weather Service.

6. References

Armijo, L., 1969: A Theory for the Determination of Wind and Precipitation Velocities with Doppler Radars. *J. Atmos. Sci.,* 26, pp. 570-573

Bougeault, P., P. Binder, A. Buzzi, R. Dirks, R. A. Houze Jr, R. Kuettner, R. B. Smith, R. Steinacker and H. Volkert, 2001: The MAP special observing period. *Bull. Am. Meteorol. Soc.,* 82, 433-462.

Bousquet, O., and M. Chong, 1998: A multiple Doppler and continuity adjustment technique (MUSCAT) to recover wind components from Doppler radar measurements. *J. Atmos. Oceanic Technol.*, 15, 343-359.

Bousquet, O., and M. Chong, 2000: The oceanic mesoscale convective system and associated mesovortex observed on 12 December 1992 during TOGA COARE. *Quart. J. Roy. Meteor. Soc.,* 126, 189-212.

Bousquet, O., and B. F. Smull, 2003: Airflow and precipitation fields within deep Alpine valleys observed by airborne radar. *J. of Appl. Meteorol.*, 42, 1497-1513

Bousquet, O., and B. F. Smull, 2006: Observed mass transports accompanying upstream orographic blocking during MAP IOP8, *Quart. J. Roy. Meteor. Soc.,* 132, 2393-2413.

Bousquet, O., P. Tabary, and J. Parent du Châtelet, 2007: On the value of operationally synthesized multiple-Doppler wind fields, *Geophys. Res. Lett.*, *34*, L22813, doi:10.1029/2007GL030464.

Bousquet, O., P. Tabary, and J. Parent du Châtelet, 2008a: Operational multiple-Doppler wind retrieval inferred from long range radar velocity measurements, *J. Appl. Meteorol. Clim.,* 47, 2929–2945.

Bousquet, O., T. Montmerle, and P. Tabary, 2008b: Using operationally synthesized multiple-Doppler winds for high resolution NWP model horizontal wind verification. *Geophys. Res. Lett.*, *35*, L10803, doi:10.1029/2008GL033975.

Bousquet, O., 2009: Dynamical and microphysical properties of high impact orographic mesoscale convective systems from high resolution operational multiple-Doppler and polarimetric radar data. *Preprints*, 34th Conference on Radar Meteorology, Williamsburg, USA

Browning, K.A., and R. Wexler, 1968: The determination of kinematic properties of a wind field using Doppler radar, *J. Appl. Meteorol., 7,* 105–113.

Browning, K.A., 1999: Mesoscale aspects of extratropical cyclones: An observational perspective. in *Life Cycles of Extratropical Cyclones*, American Meteorological Society, Boston, 265-283.

Browning, K.A., 2004: The sting at the end of the tail: Damaging winds associated with extratropical cyclones. *Quart. J. Roy. Meteor. Soc.*, 130, 375-399.

Chong, M., and J. Testud, 1996: Three-Dimensional Air Circulation in a Squall Line from Airborne Dual-Beam Doppler Radar Data: A Test of Coplane Methodology Software. *J. Atmos. Oceanic Technol.,* 13, 36-53.

Chong, M., and O. Bousquet, 2001: On the application of Muscat to a ground-based dual-Doppler radar system., *Meteorol. Atmos. Phys.,* 78, 133-139.

Chong, M., J.-F. Georgis, O. Bousquet, S. R. Brodzik, C. Burghart, S. Cosma, U. Germann, V. Gouget, R. A. Houze Jr., C. N. James, S. Prieur, R. Rotunno, F. Roux, J. Vivekanandan, Z.-X. Zeng, 2000: Real–Time Wind Synthesis from Doppler Radar Observations during the Mesoscale Alpine Programme. *Bull. Amer. Meteor. Soc.*, 81, 2953–2962.

Delrieu, G., and co-authors, 2005: The Catastrophic Flash-Flood Event of 8–9 September 2002 in the Gard Region, France: A First Case Study for the Cévennes–Vivarais Mediterranean Hydrometeorological Observatory. *Journal of Hydrometeorology,* 6, 34-52.

Doviak, R. J., and D. S. Zrnic, 1993: Doppler radar and weather observations (second edition), Academic Press, Inc.

Drechsel, S., G. J. Mayr, M. Chong, M. Weissmann, A. Dörnbrack, and R. Calhoun, 2009: Three-dimensional wind retrieval: application of MUSCAT to dual-doppler lidar. *J. Atmos. Oceanic Technol.*, 26, 635–646.

Gamache, J. F., 1995: A three-dimensional variational method for determining wind velocities from Doppler data as applied to the TOGA COARE test case. Summary Report, TOGA COARE Int. Data Workshop TOGA, COARE International Project Office, UCAR, Boulder, CO, 106 pp.

Gao, J., M. Xue, A. Shapiro and K. K. Droegemeier, 1999: A Variational Method for the Analysis of Three-Dimensional Wind Fields from Two Doppler Radars. *Mon. Wea. Rev.*, 127, 2128-2142.

Heymsfield, G. M., 1978: Kinematic and Dynamic aspects of the Harrah tornadic storm analyzed from dual-Doppler radar data. Mon. Wea. Rev., 106, 253-264.

Lhermitte, R. M., and L. J. Miller, 1970: Doppler radar methodology for the observation of convective storms. *Preprints, 14th Radar Meteorology Conf*, Tucson, Arizona, Amer. Meteorol. Soc, pp 133-138.

Georgis, J-F., F. Roux, M. Chong and S. Pradier, 2003: Triple-Doppler analysis of the heavy rain event observed in the Lago Maggiorre region during MAP IOP 2b. *Quart. J. Roy. Meteor. Soc.*, 129, 495-522.

Montmerle, T., and C. Faccani, 2009: Mesoscale assimilation of radial velocities from Doppler radar in a pre-operational framework. *Mon. Wea. Rev.*,137, 1939–1953.

O'Brien, J. J., 1970: Alternative solutions to the classical vertical velocity problem., *J. Appl. Meteor.*, 9, 197-203.

Radnóti, G., R. Ajjaji, R. Bubnovà, M. Caian, E. Cordoneanu, K. von der Emde, J.-D. Gril, J. Hoffman, A. Horànyi, S. Issara, V. Ivanovici, M. Janousek, A. Joly, P. Le Moigne, S.

Malardel, 1995 : The spectral limited area model Arpege/Aladin. *PWPR Report Series* n° 7, WMO T.D. N. 799, 111-118.

Reasor, P. D., M. D. Eastin, and J. F. Gamache, 2009: Rapidly intensifying Hurricane Guillermo (1997). Part I: Low-wavenumber structure and evolution. *Mon. Wea. Rev.*, 137, 603–631.

Reeves, H. D., and Y-L Lin, 2005: Effect of stable layer formation over the Po Valley on the development of convection during MAP IOP-8. *J. Atmos. Sci.*, 63, 2567-2584.

Scialom, G., and Y. Lemaître, 1990 : A New Analysis for the Retrieval of Three-Dimensional Mesoscale Wind Fields from Multiple Doppler Radar. *J. Atmos. Oceanic Technol.*, 7, 640-665

Shapiro, M. A., and D. Keyser, 1990: Fronts, jet streams and the tropopause. *Extratropical Cyclones, The Erik Palmén Memorial Volume,* C. W. Newton and E. O. Holopainen, Eds., Amer. Meteor. Soc., 167-191.

Schultz, D. M., D. Keyser and L. Bosart, 1998: The Effect of Large-Scale Flow on Low-Level Frontal Structure and Evolution in Midlatitude Cyclones. *Mon. Wea. Rev.*, 126, pp. 1767-1791

Steiner, M., O. Bousquet, R. A. Houze Jr, B. F. Smull, and M. Mancini, 2003: Airflow within major Alpine river valleys under heavy rainfall. *Quart. J. Roy. Meteor. Soc.,* 129, 411-432.

Sugier, J., J. Parent-du-Châtelet, P. Roquain, and A. Smith, 2002: Detection and removal of clutter and anaprop in radar data using a statistical scheme based on echo fluctuation. *Proc. Second European Radar Conf.*, Delft, Netherlands, Copernicus GmbH, 17–24.

Tabary, P., F. Guibert, L. Perier, and J. Parent-du-chatelet, 2006: An operational triple-PRT scheme for the French radar network. *J. Atmos. Oceanic Technol.*, 23, 1645-1656.

Tabary, P., A.A. Boumahmoud, H. Andrieu, R. J. Thompson, A. J. Illingworth, E. Le Bouar and J. Testud, 2011: Evaluation of two "integrated" polarimetric Quantitative Precipitation Estimation (QPE) algorithms at C-band, *Journal of Hydrology*, 405., 248,260.

Tuttle, J. D., and G. B. Foote, 1990: Determination of boundary layer airflow from a single Doppler radar. *J. Atmos. Oceanic Technol.*, 7, 218–232.

Wernli, H., Dirren, S., Liniger, M. A. and Zillig, M., 2002, Dynamical aspects of the life cycle of the winter storm 'Lothar' (24–26 December 1999). *Quart. J. Roy. Meteor. Soc*, 128, 405-429

Zrnic, D. S., and P. Mahapatra, 1985: Two methods of ambiguity resolution in pulsed Doppler weather radars., *IEEE Trans. Aerosp. Electron. Syst.,* 21, 470–483.

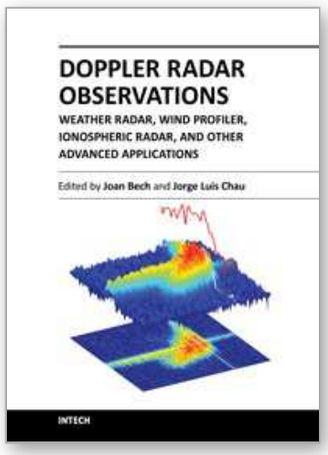

Doppler Radar Observations - Weather Radar, Wind Profiler, Ionospheric Radar, and Other Advanced Applications

Edited by Dr. Joan Bech

ISBN 978-953-51-0496-4
Hard cover, 470 pages
Publisher InTech
Published online 05, April, 2012
Published in print edition April, 2012

Doppler radar systems have been instrumental to improve our understanding and monitoring capabilities of phenomena taking place in the low, middle, and upper atmosphere. Weather radars, wind profilers, and incoherent and coherent scatter radars implementing Doppler techniques are now used routinely both in research and operational applications by scientists and practitioners. This book brings together a collection of eighteen essays by international leading authors devoted to different applications of ground based Doppler radars. Topics covered include, among others, severe weather surveillance, precipitation estimation and nowcasting, wind and turbulence retrievals, ionospheric radar and volcanological applications of Doppler radar. The book is ideally suited for graduate students looking for an introduction to the field or professionals intending to refresh or update their knowledge on Doppler radar applications.

How to reference
In order to correctly reference this scholarly work, feel free to copy and paste the following:

Olivier Bousquet (2012). Retrieving High Resolution 3-D Wind Vector Fields from Operational Radar Networks, Doppler Radar Observations - Weather Radar, Wind Profiler, Ionospheric Radar, and Other Advanced Applications, Dr. Joan Bech (Ed.), ISBN: 978-953-51-0496-4, InTech, Available from: http://www.intechopen.com/books/doppler-radar-observations-weather-radar-wind-profiler-ionospheric-radar-and-other-advanced-applications/retrieving-high-resolution-3-d-wind-vector-fields-from-operational-radar-networks

INTECH
open science | open minds

InTech Europe
University Campus STeP Ri
Slavka Krautzeka 83/A
51000 Rijeka, Croatia
Phone: +385 (51) 770 447
Fax: +385 (51) 686 166
www.intechopen.com

InTech China
Unit 405, Office Block, Hotel Equatorial Shanghai
No.65, Yan An Road (West), Shanghai, 200040, China
中国上海市延安西路65号上海国际贵都大饭店办公楼405单元
Phone: +86-21-62489820
Fax: +86-21-62489821

© 2012 The Author(s). Licensee IntechOpen. This is an open access article distributed under the terms of the Creative Commons Attribution 3.0 License, which permits unrestricted use, distribution, and reproduction in any medium, provided the original work is properly cited.

IntechOpen

IntechOpen